

ISO-LWS spectroscopy of Centaurus A: extended star formation

S. J. Unger¹, P. E. Clegg¹, G. J. Stacey², P. Cox³, J. Fischer⁴, M. Greenhouse⁵, S. D. Lord⁶, M. L. Luhman⁴, S. Satyapal⁵, H. A. Smith⁷, L. Spinoglio⁸, and M. Wolfire⁹

¹ Physics Dept., Queen Mary & Westfield College, University of London, London E1 4NS, U.K.

² Cornell University, Ithaca, NY, USA

³ Institut d'Astrophysique Spatiale, Orsay, France

⁴ Naval Research Laboratory, Washington, USA

⁵ NASA Goddard, Greenbelt, USA

⁶ IPAC, California Institute of Technology, Pasadena, USA

⁷ Harvard-Smithsonian Center for Astrophysics, Cambridge, MA, USA

⁸ Istituto di Fisica dello Spazio Interplanetario-CNR, Roma, Italy

⁹ University of Maryland, College Park, MD, USA

Received ;Accepted

Abstract. We present the first full FIR spectrum of Centaurus A (NGC 5128) from 43 - 196.7 μm . The data was obtained with the ISO Long Wavelength Spectrometer (LWS). We conclude that the FIR emission in a 70'' beam centred on the nucleus is dominated by star formation rather than AGN activity. The flux in the far-infrared lines is $\sim 1\%$ of the total FIR: the [C II] line flux is $\sim 0.4\%$ FIR and the [O I] line is $\sim 0.2\%$, with the remainder arising from [O III], [N II] and [N III] lines. These are typical values for starburst galaxies.

The ratio of the [N III] / [N II] line intensities from the HII regions in the dust lane corresponds to an effective temperature, $T_{\text{eff}} \sim 35500$ K, implying that the tip of the main sequence is headed by O8.5 stars and that the starburst is $\sim 6 \times 10^6$ years old. This suggests that the galaxy underwent either a recent merger or a merger which triggered a series of bursts. The N/O abundance ratio is consistent with the range of $\sim 0.2 - 0.3$ found for Galactic HII regions.

We estimate that $< 5\%$ of the observed [C II] arises in the cold neutral medium (CNM) and that $\sim 10\%$ arises in the warm ionized medium (WIM). The main contributors to the [C II] emission are the PDRs, which are located throughout the dust lane and in regions beyond where the bulk of the molecular material lies. On scales of ~ 1 kpc the average physical properties of the PDRs are modelled with a gas density, $n \sim 10^3 \text{ cm}^{-3}$, an incident far-UV field, $G \sim 10^2$ times the local Galactic field, and a gas temperature of ~ 250 K.

Key words: Galaxies: individual: Centaurus A = NGC 5128 – Infrared: galaxies – Galaxies: active, ISM, starburst

1. Introduction

Centaurus A (NGC 5128) is the nearest ($d = 3.5$ Mpc; $1'' \sim 17$ pc, Hui et al. 1993) example of a giant elliptical galaxy associated with a powerful radio source. The large-scale radio morphology consists of twin radio lobes separated by ~ 5 degrees on the sky. The compact (\sim milliarcsecond) radio nucleus is variable and has a strong jet extending ~ 4 arcminutes towards the northeast lobe. The spectacular optical appearance is that of a giant elliptical galaxy that appears enveloped in a nearly edge on, warped dust lane. There is also a series of faint optical shells. The stellar population in the dominant elliptical structure is old, whilst that of the twisted dust lane is young, sporadically punctuated by HII regions, dust and gas (Graham 1979). The overall structure of Cen A resembles that of a recent ($< 4 \times 10^8$ years, Tubbs 1980) merger, between a spiral and a large elliptical galaxy. The dust lane is the source of most (90 %) of the far-infrared luminosity ($L_{\text{FIR}} \sim 3 \times 10^9 L_{\odot}$) and is thought to be re-radiated starlight from young stars in the dusty disk (Joy et al. 1988).

In Sect. 2 we describe the observations and data analysis. Sect. 3 looks at the general FIR properties and proceeds to model the HII regions and the PDRs in the dust lane. Sect. 4 summarises the results and presents our conclusions.

2. Observations

Cen A was observed with the LWS grating ($R = \lambda/\Delta\lambda \sim 200$) as part of the LWS consortium's guaranteed time extragalactic programme. A full grating observation (43 - 196.7 μm) was taken of the nucleus at the centre of the dust lane and a series of line observations were taken at two positions in the SE and NW regions of the dust lane. A short [C II] 157 μm line observation was taken off-source at position #4 (see Table 1) to estimate the Galactic emission near the source. Position #1 was intended to provide a deeper integration coincident with position #2, but was accidentally offset.

A series of half-second integration ramps were taken at each grating position with four samples per resolution element ($\Delta\lambda = 0.29 \mu\text{m}$ $\lambda\lambda 43 - 93 \mu\text{m}$ and $\Delta\lambda = 0.6 \mu\text{m}$ $\lambda\lambda 84 - 196 \mu\text{m}$). The total integration time per resolution element and per pointing were: position #1 88 s for the [O III] 52 μm and 34 s for the [N III] 57 μm ; position #2 (the centre), 30 s for the range 43–196 μm ; positions NW and SE (2 point raster map) 22 s for the the [O I] 63 μm , 14 s for the [O III] 88 μm , 12 s for the [N II] 122 μm , 28 s for the [O I] 145 μm and 12 s for the [C II] 158 μm ; position #4 12 s for the [C II] 158 μm .

The data were processed with RAL pipeline 7 and analysed using the LIA and ISAP packages. The LWS flux calibration and relative spectral response function (RSRF) were derived from observations of Uranus (Swinyard et al. 1998). The full grating spectrum at the centre enabled us to estimate the relative flux uncertainty between individual detectors arising from uncertainties in the relative responsivity and the dark-current subtraction. The offsets between the detectors (excluding detector SW1) was $\leq 10\%$. The [O III] 88 μm line on detectors SW5 and LW1 had a 15 % systematic uncertainty and the [C II] line on detectors LW3 and LW4 had a 10 % systematic uncertainty. We therefore adopt a relative flux uncertainty of $\sim 15\%$. Because we only took spectra of individual lines at the NW and SE positions there is no corresponding overlap in wavelength coverage at these positions. One indicator of relative flux uncertainty is a discrete step down in flux, of $\sim 25\%$, at $\sim 125 \mu\text{m}$ at the SE position. The relative flux uncertainty is assumed to be $\leq 25\%$ at these positions.

The absolute flux calibration w.r.t. Uranus for point like objects observed on axis is better than 15 % (Swinyard et al. 1998). However, extended sources give rise either to channel fringes or to a spectrum that is not a smooth function of wavelength. This is still a calibration issue. For example, in Fig. 2, detectors SW5, LW1, LW2 have slopes that differ from those of their neighbours in the overlap region. This may account for the continuum shape, which is discussed in Sect. 3.1. The LWS beam profile is known to be asymmetric and is still under investigation. We therefore adopt a value for the FWHM of 70'' at all wavelengths, believing that a more sophisticated treatment would not significantly affect our conclu-

sions. We also note that there is good cross calibration between the ISO-LWS results and the Far-infrared Imaging Fabry-Perot Interferometer (FIFI) (Madden et al. 1995); the [C II] peak fluxes agree to within $\sim 10\%$.

Table 1. Observation Log

Position	Offset in RA arcsec	Offset in Dec arcsec	Date/AOT
#1	+ 29	- 12	1996 Aug 23 L02
#2 Centre	0	0	1997 Aug 11 L01
#3 (map)			1997 Feb 12 L02
NW	- 53	+ 27	
SE	+ 110	- 49	
#4 (off)	- 2	+ 600	1997 Feb 12 L02
Offsets w.r.t. 13h 25m 27.6s -43d 01'08.6''J2000			

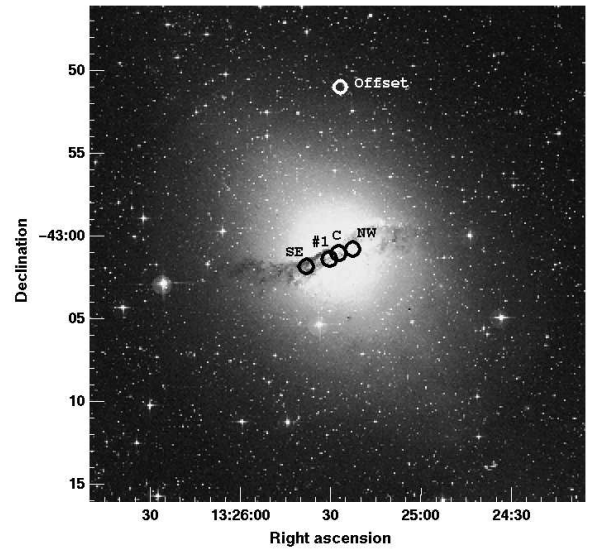


Fig. 1. Cen A digital sky survey image overlaid with the LWS beam positions

3. Results and discussion

3.1. General FIR properties

The far-infrared continuum at each position is modelled with a single-temperature blackbody spectrum of the form $F_\lambda \propto \Omega B_\lambda(T)(1-e^{-\tau_{\text{dust}}})$, where the solid angle, Ω , is constrained to equal the LWS beam, $B_\lambda(T)$ is the Planck

function at temperature T and $\tau_{\text{dust}} \propto \lambda^{-1.5}$. The result for the central position is shown as the dashed curve in Fig. 2. Although the observed continuum is not a simple function of wavelength and the single temperature blackbody is not an especially good fit, particularly at wavelengths $> 100 \mu\text{m}$, a better calibration of straylight and the beam profile is required for anything more sophisticated. The best FIR temperature at each position is ~ 30 K.

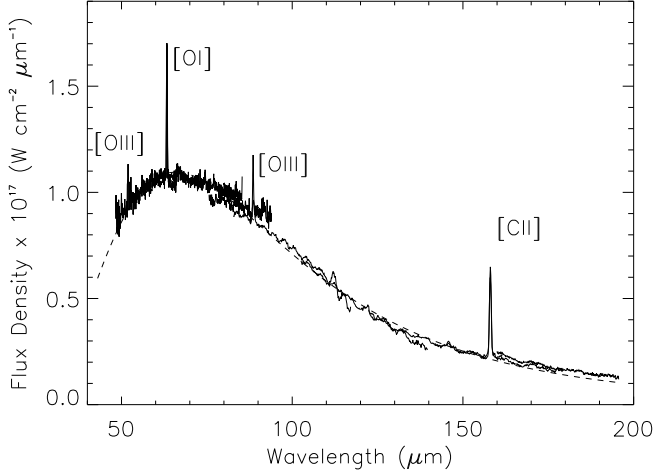


Fig. 2. LWS spectrum of the central region of the dust lane (dashed line is the blackbody fit)

The luminosities quoted here are derived from the line fluxes listed in Table 2. At the central position, the total luminosity in all of the far-infrared lines is $2.6 \times 10^7 L_{\odot}$, which is $\sim 1\%$ of the total FIR luminosity ($L_{43-197 \mu\text{m}} = 3.2 \times 10^9 L_{\odot}$). The $[\text{C II}]$ luminosity is $1.1 \times 10^7 L_{\odot}$ (0.4 % FIR) and the $[\text{O I}]$ luminosity is $7.5 \times 10^6 L_{\odot}$ (0.2 % FIR). Because full spectra are not available at the NW and SE positions we estimate the FIR continuum luminosity by integrating under the single-temperature blackbody fit to the data. At the NW position the total FIR luminosity, $L_{43-197 \mu\text{m}} = 2.2 \times 10^9 L_{\odot}$. The $[\text{C II}]$ luminosity is $9.3 \times 10^6 L_{\odot}$ (0.4 % FIR) and the $[\text{O I}]$ luminosity is $3.4 \times 10^6 L_{\odot}$ (0.2 % FIR). At the SE position the total FIR luminosity, $L_{43-197 \mu\text{m}} = 8.7 \times 10^8 L_{\odot}$. The $[\text{C II}]$ luminosity is $3.5 \times 10^6 L_{\odot}$ (0.4 % FIR) and the $[\text{O I}]$ luminosity is $2.0 \times 10^6 L_{\odot}$ (0.2 % FIR). These are typical values for starburst galaxies (c.f. Lord et al. 1996).

3.2. Ionized gas lines

Photons of energy 35.12, 29.60 and 14.53 eV are required to form O^{++} , N^{++} and N^{+} , respectively, so that the observed $[\text{O III}]$, $[\text{N III}]$ and $[\text{N II}]$ emission must originate in

or around HII regions. The $[\text{O III}]$ line ratio is a sensitive function of density in the range $\sim 30 - 10^4 \text{ cm}^{-3}$. For the central position this ratio is ~ 0.9 , corresponding to an electron density, $n_e \sim 100 \text{ cm}^{-3}$ (Rubin et al. 1994). The $[\text{O III}]$ lines indicate a higher electron density, $n_e \sim 250 \text{ cm}^{-3}$, for the starburst nuclei of M82 (Colbert et al. 1999) and M83 (Stacey et al. 1999). In contrast, the $[\text{N II}]$ 205 μm / 122 μm line intensity ratio for the Galaxy gives an average electron density, of only $\sim 3 \text{ cm}^{-3}$ (Petuchowski & Bennett 1993). The *thermal pressure* of the ionized material in the Cen A dust lane is therefore closer to that of starburst galaxies than to that of the Milky Way.

Since the $[\text{N III}]$ 57 μm and the $[\text{N II}]$ 122 μm lines arise from different ionization states of the same element, the line intensity ratio is sensitive to the hardness of the interstellar UV field and therefore to the spectral type of the hottest main sequence star. For the central position $[\text{N III}] / [\text{N II}] \sim 1.6$. This is larger than the value of ~ 0.9 for M83 (Stacey et al. 1999) but smaller than the value of ~ 2.1 for M82 (Colbert et al. 1999). Assuming that the region is ionization bounded, with an electron density, $n_e \sim 100 \text{ cm}^{-3}$ the $[\text{N III}] / [\text{N II}]$ line intensity ratio for Cen A corresponds to an abundance ratio $\text{N}^{++}/\text{N}^{+}$ of ~ 0.3 ; this corresponds to an effective temperature, $T_{\text{eff}} \sim 35\,500$ K (Rubin et al. 1994). Applying the same corrections to M82 and M83 with $n_e \sim 250 \text{ cm}^{-3}$ implies an effective temperature, $T_{\text{eff}} \sim 34\,500$ K for M83 and $T_{\text{eff}} \sim 35\,500$ K for M82. If the effective temperature in Cen A corresponds to the tip of the main sequence formed in a single starburst, we are observing O8.5 stars and the burst is $\sim 6 \times 10^6$ years old. If the burst was triggered by the spiral-elliptical galaxy merger then its occurrence was very recent. Alternatively, the merger triggered a series of bursts of star formation, of which we are witnessing the most recent.

The N^{++} and O^{++} coexist in roughly the same ionization zones, and the $[\text{O III}]$ 52 μm and $[\text{N III}]$ 57 μm lines have roughly the same critical density. As a result the ratio of these lines is an indicator, to within $\sim 50\%$, of the $\text{N}^{++}/\text{O}^{++}$ abundance ratio, which itself, is nearly equal to the N/O ratio in the hard UV field environments we are seeing here (Rubin et al. 1988). The line ratio we observe at the centre of the dust lane is ~ 0.3 - the same as found in the nucleus of M82 (Colbert et al. 1999), but much smaller than that found for the nucleus of M83 (~ 0.67 Stacey et al. 1999).

A more precise determination of the abundance ratio requires the observed line ratio to be divided by the volume emissivity ratio. The latter ratio is dependent on the electron density because the two lines have slightly different critical densities. Using our value for the electron density $\sim 100 \text{ cm}^{-3}$ and Fig. 3 of Lester et al. (1987) we estimate that the N/O abundance ratio to be ~ 0.2 in Cen A. This value is consistent with the range of $\sim 0.2 - 0.3$ found for Galactic HII regions (Rubin et al. 1988). The nitrogen to oxygen abundance ratio is a measure of the

Table 2. Line Fluxes

Line	λ_{rest} μm	#1 Flux	Centre Flux	NW Flux	SE Flux
[O III] 3p2-3p1	51.815	0.31	0.72	-	-
[N III] 2p $\frac{3}{2}$ -2p $\frac{1}{2}$	57.3170	0.16	0.24	-	-
[O I] 3p1-3p2	63.184	-	1.96	0.90	0.51
[O III] 3p1-3p0	88.356	-	0.70	0.6	0.2
[N II] 3p2-3p1	121.898	-	0.15	0.15	≤ 0.15
[O I] 3p0-3p1	145.525	-	0.11	0.08	≤ 0.03
[C II] 2p $\frac{3}{2}$ -2p $\frac{1}{2}$	157.741	-	2.91	2.43	0.92

Flux $\times 10^{-18} \text{ W cm}^{-2}$

- wavelength range not covered

upper limits are 3 x rms residuals from a fit to the continuum

[C II] 157 μm flux at #4 (off) is 0.04

chemical evolution and we expect it to increase with time (cf. the solar value of ~ 0.12).

3.3. Neutral gas lines

Carbon has a low ionization potential (11.4 eV), which is less than that of hydrogen. [C II] 157 μm line emission is therefore observed from both neutral and ionized hydrogen clouds. We model the [C II] line emission with three components: Photodissociation regions (PDRs) on the surfaces of UV exposed molecular clouds; cold ($T \sim 100 \text{ K}$) HI clouds (i.e. the cold neutral medium (CNM) Kulkarni & Heiles 1987, Wolfire et al. 1995); and diffuse HII regions (i.e. the warm ionized medium (WIM) Heiles 1994).

3.3.1. HI clouds

It can be shown that the intensity in the [C II] line emitted from gas clouds with density, $n(\text{H})$ and temperature (T) is given by (c.f. Madden et al. 1993)

$$I_{\text{C}^+} = 2.35 \times 10^{-21} \left[\frac{2\exp(\frac{-91.3}{T})}{1 + 2\exp(\frac{-91.3}{T}) + \frac{n_{\text{crit}}}{n_{\text{H}}}} \right] X_{\text{C}^+} N(\text{HI}) \quad (1)$$

where the critical density for collisions with H, $n_{\text{crit}} \sim 3000 \text{ cm}^{-3}$ (Launay & Roueff 1977) and the fractional C^+ relative to hydrogen is $X_{\text{C}^+} \sim X_{\text{C}} = 1.4 \times 10^{-4}$ (Sofia et al. 1997).

$N(\text{HI})$ is estimated from the HI 21cm map of Van Gorkom et al. (1990) to be $18.8 \times 10^{20} \text{ atom cm}^{-2}$ at the SE position. The central and NW positions are difficult to estimate due to HI absorption against the nuclear continuum. There may be a central hole in the HI and the column density is certainly not higher than the peak observed in the SE region of the dust lane (Van Gorkom et al. 1990)

Assuming typical Galactic values for the temperature, $T \sim 80 \text{ K}$, and hydrogen density, $n \sim 30 \text{ cm}^{-3}$, results in an estimated [C II] flux of $3.5 \times 10^{-20} \text{ W cm}^{-2}$ in a 70'' LWS beam at the SE position. This corresponds to 4 %, 1 % and 1 % of the observed [C II] flux at positions SE, Centre and NW respectively. The peak HI emission line flux corresponds to $1.9 \times 10^{-19} \text{ W cm}^{-2}$ which is only 6 % and 8 % of the [C II] flux at the centre and NW positions respectively. We conclude that there is very little [C II] emission in our beams from HI clouds.

3.3.2. Diffuse HII regions

Ionized carbon can be found in both neutral gas and ionized gas clouds, and is an important coolant for each. We detected [O III] 88 μm in all 3 beam positions so there is an ionized gas component in each beam. Using the constant density HII region model of Rubin (1985) with the Kurucz abundances, 10^{49} ionizing photons per second and our derived density, $n_e \sim 100 \text{ cm}^{-3}$ and effective temperature, $T_{\text{eff}} \sim 35500 \text{ K}$ we can estimate the [C II] emission from the HII regions. Applying the model [O III] 88 μm / [C II] 158 μm line ratio of 0.35 to the observed [O III] 88 μm line flux at each position results in ~ 10 % contribution to the observed [C II] line flux in each beam. Scaling the model fluxes to the distance of Cen A gives ~ 3000 HII regions in the central and NW regions and ~ 1000 HII regions in the SE region.

The estimate above assumes that the observed lines have the same filling factor in the large LWS beam. If, alternatively, we were to assume that the ionized component was instead dominated by a contribution from an extended low density warm ionized medium (ELDWIM) with $n_e \sim 3 \text{ cm}^{-3}$, then the [C II] flux can be estimated from the ratio of the [C II] / [N II] lines to be ~ 18 % at the central position. The observations of the [N II] 121.9 μm line at the NW and SE positions (with lower signal to

noise) indicate a similar fractional component (21 % and ≤ 56 %, respectively).

We have estimated the density in the HII regions in the centre of Cen A to be $\sim 100 \text{ cm}^{-3}$ with an effective temperature, $T_{\text{eff}} \sim 35500 \text{ K}$. Based on the HII region models of Rubin (1985) we estimate that ~ 10 % of the observed [C II] arises in the WIM.

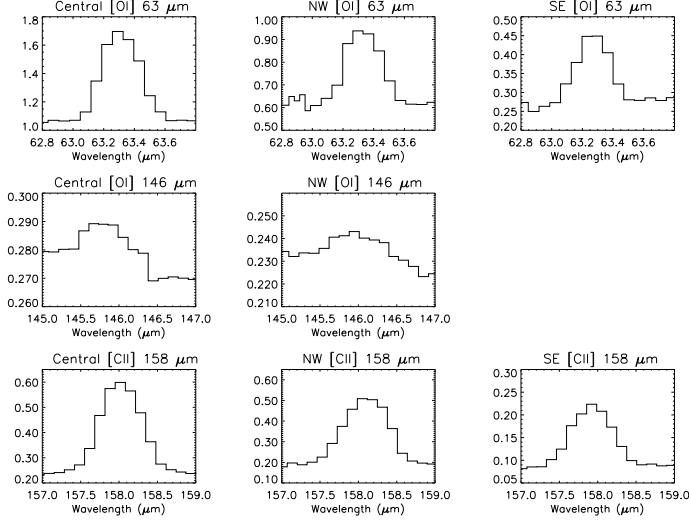


Fig. 3. PDR Lines (Flux Density $\times 10^{17} \text{ W cm}^{-2} \mu\text{m}^{-1}$). Note the [C II] lines are the total observed flux density i.e. PDR + CNM + WIM

3.3.3. PDRs

Far-UV photons ($6 \text{ eV} < h\nu \leq 13.6 \text{ eV}$) from either O/B stars or an AGN will photo-dissociate H_2 and CO molecules and photo-ionize elements with ionization potentials less than the Lyman limit (e.g. C^+ ionization potential = 11.26 eV). The gas heating in these photodissociation regions (PDRs) is dominated by electrons ejected from grains due to the photoelectric effect. Gas cooling is dominated by the emission of [O I] $63 \mu\text{m}$ and [C II] $158 \mu\text{m}$ emission. Observations of these lines, the [O I] $146 \mu\text{m}$ and CO ($J=1-0$) 2.6 mm lines and the FIR continuum can be used to model the average physical properties of the neutral interstellar medium (Wolfire et al. 1990). Kaufman et al. (1999) have computed PDR models over a wide range of physical conditions. The new code accounts for gas heating by small grains/PAHs and large molecules, and uses a lower, gas phase carbon abundance ($X_{\text{C}} = 1.4 \times 10^{-4}$, Sofia et al. 1997) and oxygen abundance ($X_{\text{O}} = 3.0 \times 10^{-4}$, Meyer et al. 1998). The [O I] $63 \mu\text{m}$ / [C II] $158 \mu\text{m}$ line ratio and either the [O I] $146 \mu\text{m}$ / [O I] $63 \mu\text{m}$ line ratio or the ([O I] $63 \mu\text{m}$ + [C II] $158 \mu\text{m}$) /

FIR continuum can be used as PDR diagnostics to determine the average gas density (i.e the proton density, $n \text{ cm}^{-3}$), the average incident far-UV flux (in units of the Milky Way flux, $G_0 = 1.6 \times 10^{-3} \text{ erg cm}^{-2} \text{ s}^{-1}$) and the gas temperature.

We assume that the measured [C II] flux at each position should have ~ 10 % subtracted, due to the HI and WIM components, before it is used to model the PDRs (if, alternatively, a 20 % ELDWIM contribution is subtracted it would not significantly affect the PDR parameters derived below). The PDR lines are plotted in Fig. 3 and the line intensity ratios are given in Table 3.

Table 3. PDR diagnostic line intensity ratios

Line Ratio	Centre	NW	SE
[O I] $63 \mu\text{m}$ / [C II] $158 \mu\text{m}$	0.7	0.4	0.6
[O I] $146 \mu\text{m}$ / [O I] $63 \mu\text{m}$	0.06	0.09	≤ 0.06
([O I] $63 \mu\text{m}$ + [C II] $158 \mu\text{m}$) / FIR	0.006	0.005	0.006

The results for the three regions are consistent with each other, having a gas density, $n \sim 10^3 \text{ cm}^{-3}$, and an incident far-UV field, $G \sim 10^2$.

At the NW position, only the combination of the [O I] $63 \mu\text{m}$ / [C II] $158 \mu\text{m}$ ratio and the ([O I] $63 \mu\text{m}$ + [C II] $158 \mu\text{m}$) / FIR continuum ratio gives a meaningful solution for G and n . The [O I] $146 \mu\text{m}$ line is clearly detected but with a very rippled baseline due to channel fringes. The observed [O I] $146 \mu\text{m}$ line flux would need to be reduced by ~ 60 % in order to obtain a consistent result with the [O I] $146 \mu\text{m}$ / [O I] $63 \mu\text{m}$ line ratio predicted by the PDR model.

The LWS results for the nucleus confirm those previously derived from IR, submm and CO observations. The consistent set of derived PDR conditions for all three positions suggest that the observed FIR emission in a $70''$ beam centred on the nucleus is dominated by star formation and not AGN activity. Joy et al. (1988) mapped Cen A at 50 and $100 \mu\text{m}$ on the KAO. They concluded that the extended FIR emission was from dust grains heated by massive young stars distributed throughout the dust lane, not the compact nucleus. Hawarden et al. (1993) mapped Cen A at $800 \mu\text{m}$ and $450 \mu\text{m}$ with a resolution of $\sim 10''$. They attribute the large scale $800 \mu\text{m}$ emission to thermal emission from regions of star formation embedded in the dust lane. They note that the H_2 emission within a few arcseconds of the nucleus, observed by Israel et al. (1990), indicates that significant UV radiation from the nucleus does not reach large radii in the plane of the dust lane i.e. the nuclear contribution to exciting the extended gas and dust disk is small.

Eckart et al. (1990) and Wild et al. (1997) mapped Cen A in ^{12}CO J=1-0, ^{12}CO J=2-1 and ^{13}CO J=1-0. All three maps have two peaks separated by $\sim 90''$ centred on the nucleus. It is interesting to note that our SE position only clips the lowest contours of the CO (1-0) and CO (2-1) maps of Wild et al. (1997). In spite of this the derived PDR parameters are consistent with those encompassing the bulk of the molecular emission. There must be extended low level CO (1-0) emission beyond the sensitivity limits of the Wild et al. (1997) maps. The lowest contour is 17.5 K km s^{-1} , corresponding to $M_{\text{H}_2} \sim 10^8 M_{\odot}$ if the material filled the LWS beam.

4. Summary and conclusions

We present the first full FIR spectrum from 43 - 196.7 μm of Cen A. We detect seven fine structure lines (see Table 2), the strongest being those generated in PDRs. At the central position, the total flux in the far-infrared lines is $\sim 1\%$ of the total FIR luminosity ($L_{43-197\mu\text{m}} = 3.2 \times 10^9 L_{\odot}$ for a distance of 3.5 Mpc). The [C II] line flux is $\sim 0.4\%$ FIR and the [O I] line flux is $\sim 0.2\%$ FIR. These are typical values for starburst galaxies (Lord et al. 1996). The [O III] 52 μm / [O III] 88 μm line intensity ratio is ~ 0.9 , which corresponds to an electron density, $n_e \sim 100 \text{ cm}^{-3}$ (Rubin et al. 1994). The *thermal pressure* of the ionized medium in the Cen A dust lane is closer to that of starburst galaxies ($n_e \sim 250 \text{ cm}^{-3}$ in M82 (Colbert et al. 1999) and M83 (Stacey et al. 1999)) than that of the Milky Way ($n_e \sim 3 \text{ cm}^{-3}$ (Pettuchowski & Bennett 1993)).

The [N III] / [N II] line intensity ratio is ~ 1.6 , giving an abundance ratio $\text{N}^{++}/\text{N}^{+} \sim 0.3$, which corresponds to an effective temperature, $T_{\text{eff}} \sim 35\,500 \text{ K}$ (Rubin et al. 1994). Assuming a coeval starburst, then the tip of the main sequence is headed by O8.5 stars, and the starburst is $\sim 6 \times 10^6$ years old. If the burst in Cen A was triggered by the spiral-elliptical galaxy merger then its occurrence was very recent. Alternatively, the merger triggered a series of bursts of star formation and we are witnessing the most recent activity.

We estimate that the N/O abundance ratio is ~ 0.2 in the HII regions in Cen A. This value is consistent with the range of $\sim 0.2 - 0.3$ found for Galactic HII regions (Rubin et al. 1988). N/O is a measure of the chemical evolution and we expect it to increase with time (c.f. the solar value of ~ 0.12).

We estimate that $\sim 10\%$ of the observed [C II] arises in the WIM. The CNM contributes very little ($< 5\%$) [C II] emission at our beam positions. The bulk of the emission is from the PDRs.

We derive the average physical conditions for the PDRs in Cen A for the first time. There is active star formation throughout the dust lane and in regions beyond the bulk of the molecular material. The FIR emission in the 70'' LWS beam at the nucleus is dominated by emission from star formation rather than AGN activity. On

scales of $\sim 1 \text{ kpc}$ the average physical properties of the PDRs are modelled with a gas density, $n \sim 10^3 \text{ cm}^{-3}$, an incident far-UV field, $G \sim 10^2$ and a gas temperature of $\sim 250 \text{ K}$.

Acknowledgements

Many thanks to the dedicated efforts of the LWS instrument team. The ISO Spectral Analysis Package (ISAP) is a joint development by the LWS and SWS Instrument Teams and Data Centers. Contributing institutes are CESR, IAS, IPAC, MPE, QMW, RAL and SRON.

References

- Colbert J.W., Malkan M.A., Clegg P.E., et al., 1999, ApJ 511, 721
- Eckart A., Cameron M., Rothermel H., et al., 1990, ApJ 363, 451
- Graham J., 1979, ApJ 232, 60
- Hawarden T.G., Sandell G., Matthews H.E., et al., 1993, MNRAS 260, 844
- Heiles C., 1994, ApJ 436, 720
- Hui X., Ford H.C., Ciardillo R., et al., 1993, ApJ 414, 463
- Israel F.P., van Dishoeck E.F., Baas F. et al., 1990, A&A 227, 342
- Joy M., Lester D.F., Harvey P.M., et al., 1988, ApJ 326, 662
- Kaufman M.J., Wolfire M.G., Hollenbach D., et al., 1999, ApJ in press
- Kulkarni S.R., Heiles C., 1987, in Hollenbach, D., Thronson Jr, H.A. (eds.) *Interstellar Processes*. Reidel, Dordrecht, p. 87
- Launay J.M., Roueff E., 1977, JPhysB 10, 879
- Lester D.F., Dinnerstein H.L., Werner M.W., et al., 1987, ApJ 320, 573
- Lord S.D., Malhotra S., Lim T.L., et al., 1996, A&A 315, L117
- Madden S.C., Geis N., Genzel R., et al, 1993, ApJ 407, 579
- Madden S., Geis N., Townes C.H. et al., 1995, *Airbourne Astronomy Symposium on the Galactic Ecosystem*, ASP Conf. Series 73, 181.
- Meyer D.M., Jura M., Cardelli J.A., 1998, ApJ 493, 222
- Pettuchowski S.J., Bennett C.L., 1993, ApJ 405, 591
- Rubin R.H., 1985, ApJS 57, 349
- Rubin R.H., Simpson J.P., Erickson E.F., et al., 1988, ApJ 327, 377
- Rubin R.H., Simpson J.P., Lord S.D., et al., 1994, ApJ 420, 772
- Sofia U.J., Cardelli J.A., Guerin K.P., et al., 1997, ApJ 482, L105
- Stacey G.J., Swain M.R., Bradford C.M., et al., 1999, *The Universe as seen by ISO*, ESA SP-427 p973
- Swinyard B.M., Burgdorf M.J., Clegg P.E et al., 1998, SPIE 3354

- Tubbs A.D., 1980, ApJ 241, 969
van Gorkom J.H., van der Hulst J.M., Haschick A.D., et al., 1990 AJ 99, 1781
Wild W., Eckart A., Wilkind T., 1997, A&A 322, 419
Wolfire M.G., Tielens A.G.G.M., Hollenbach D., 1990, ApJ 358, 116
Wolfire M.G., Tielens A.G.G.M., Hollenbach D., 1995, ApJ 443, 152